JOURNAL OF CATALYSIS **165,** 262–274 (1997)
ARTICLE NO. CA971468

Transient Isotopic Studies and Microkinetic Modeling of Methane Reforming over Nickel Catalysts

L. M. Aparicio

Haldor Topsøe Research Laboratories, DK-2800 Lyngby, Denmark

Received July 17, 1996; revised September 20, 1996; accepted September 20, 1996

The kinetics of elementary surface reactions involved in the reforming of methane to synthesis gas over supported nickel were studied using transient isotopic methods. To investigate methane adsorption and dehydrogenation, the reaction between CD_4 and H_2 was studied. To investigate water adsorption and dissociation, the reaction between H_2O and D_2 was studied. To investigate the formation and cleavage of C–O bonds on the nickel surface, transient CO methanation experiments were performed. Rate constants of surface elementary reactions were extracted from the data by fitting the measured response curves to microkinetic models. An overall model that describes the reactions of methane with steam and CO_2 in microkinetic terms was constructed based on these rate constants and on previously published steam reforming and CO_2 methanation data. The model suggests that there is no single rate-determining step in methane reforming with either steam or CO_2, and that under some conditions the availability of surface oxygen may play a key role in determining the rate.

INTRODUCTION

Synthesis gas production via the reforming of methane with either steam or steam/CO_2 mixtures is still the most widely employed route from natural gas to commodity chemicals:

$$CH_4 + H_2O \rightarrow CO + 3H_2$$

$$CH_4 + CO_2 \rightarrow 2CO + 2H_2.$$

Although steam reforming of natural gas has been carried out industrially since 1930, the reforming of methane is receiving renewed attention due to a widespread interest in operating with increasing amounts of CO_2 in the feed (1–20). The reason behind the trend is a desire to produce synthesis gases with lower H_2/CO ratios, better suited for downstream processes such as the oxo syntheses of aldehydes or the syntheses of methanol, acetic acid, and dimethyl ether. This last chemical may become increasingly important in coming years because of its ability to function as a clean-burning alternative fuel for diesel engines (21); if its demand increases, interest in the production of low hydrogen synthesis gas is likely to grow as well.

Methane reforming has traditionally been carried out with steam. Nonetheless, the inclusion of carbon dioxide in reformer feed has been practiced industrially for years, particularly for the production of synthesis gases destined for oxo syntheses (1, 2, 22–25). What has kept the practice from becoming too widespread is that it increases the potential for coke formation on the catalyst surface. Measures can be taken to alleviate the coke problem, and several approaches have been studied in the past. These have included the replacement of traditional nickel-based catalysts with noble metal ones (3–10, 26–28), sulfur passivation (2, 25, 29), the use of metal sulfide catalysts (20), and autothermal reforming (2, 11). Of these, only sulfur passivation and autothermal reforming are being practiced industrially, and each has its drawbacks. Noble metals are expensive, sulfur passivation and sulfide catalysts require higher operating temperatures, and autothermal reforming can only be used in conjunction with an inexpensive nitrogen-free oxygen source. The optimum solution may therefore involve the development of a nickel-based catalyst with an exceptional resistance to coke formation. This has long been recognized by several investigators, who have been studying the effect of the support and promoters on the performance of nickel catalysts, paying particular attention to coke deposition and the type of carbon deposited during reforming with carbon dioxide in the absence of steam, also known as dry reforming (10, 14–19).

The key to developing a more coke-resistant catalyst may lie in a better understanding of the methane reforming mechanism at a molecular level. For noble metal-based catalysts, information of this type has been obtained using various techniques, including isotopic tracing (4, 6) and the simultaneous monitoring of a catalyst surface and the surrounding gas phase during selected treatments with DRIFTS and mass spectroscopy (9). However, similar experiments using nickel-based catalysts have not been published. We have therefore performed a series of experiments aimed at obtaining information on the kinetics of elementary reactions occurring on a nickel catalyst's surface during reforming of methane with steam and CO_2. The experiments consisted of measuring transient responses in

0021-9517/97 $25.00

the effluent of a catalyst-loaded reactor after selected step functions were applied to the reactor inlet. The resulting response curves were fitted to kinetic models to extract rate constants of surface elementary reactions. In most cases, the switches applied to the reactor's inlet involved isotopically labeled species. For example, switches between CH_4/H_2 and CD_4/H_2 mixtures were used to study elementary reactions involved in methane adsorption and dehydrogenation. Switches between H_2 and a H_2O/D_2 mixture were used to study steam adsorption and dissociation. Transient CO methanation experiments involving steps between H_2 and CO/H_2 mixtures were used to study elementary reactions involved in C–O bond formation and cleavage on the surface. The experimental results gave a partial microkinetic picture of methane reforming. To complete the picture, an overall microkinetic model was postulated based on the results of the transient experiments, and the missing rate constants were obtained by fitting previously published kinetic data for steam reforming and the reaction of CO_2 with hydrogen.

METHODS

Materials

The catalyst used for the study contained 25 wt% Ni and was based on a $MgO–MgAl_2O_4$ support. Its BET surface area was 50 m^2/g, and its Ni surface area, determined by H_2S chemisorption (1), was 5.7 m^2/g. Catalyst particles in the size range from 0.3 to 0.8 mm were used in the study.

Premixed gases were purchased from commercial suppliers. Their purity was checked by mass spectroscopy. In the case of the CD_4/H_2 mixture, a nonnegligible water impurity was detected, and a molecular sieve trap was therefore installed on that line. To obtain a H_2O/D_2 mixture, deuterium was bubbled through a saturator containing distilled, deionized H_2O immersed in a bath thermostated at 30°C.

Experimental Setup

A schematic diagram of the apparatus used is shown in Fig. 1. The setup permitted the establishment of two parallel flows, one through a bypass and one through a recirculating reactor system. An arrangement of five computer-controlled valves determined which flow went to the recirculating reactor system and which to the bypass. Step functions in the reactor inlet were created without dead volumes by simultaneously switching these valves, four of which were 3-port bellows valves in which one port may either be connected to or isolated from the other two, and one of which was a 4-way valve. The reactor effluent was monitored before and after such switches with a mass spectrometer. In all the experiments, the flows through the reactor system and the bypass were both set at 50 ml/min

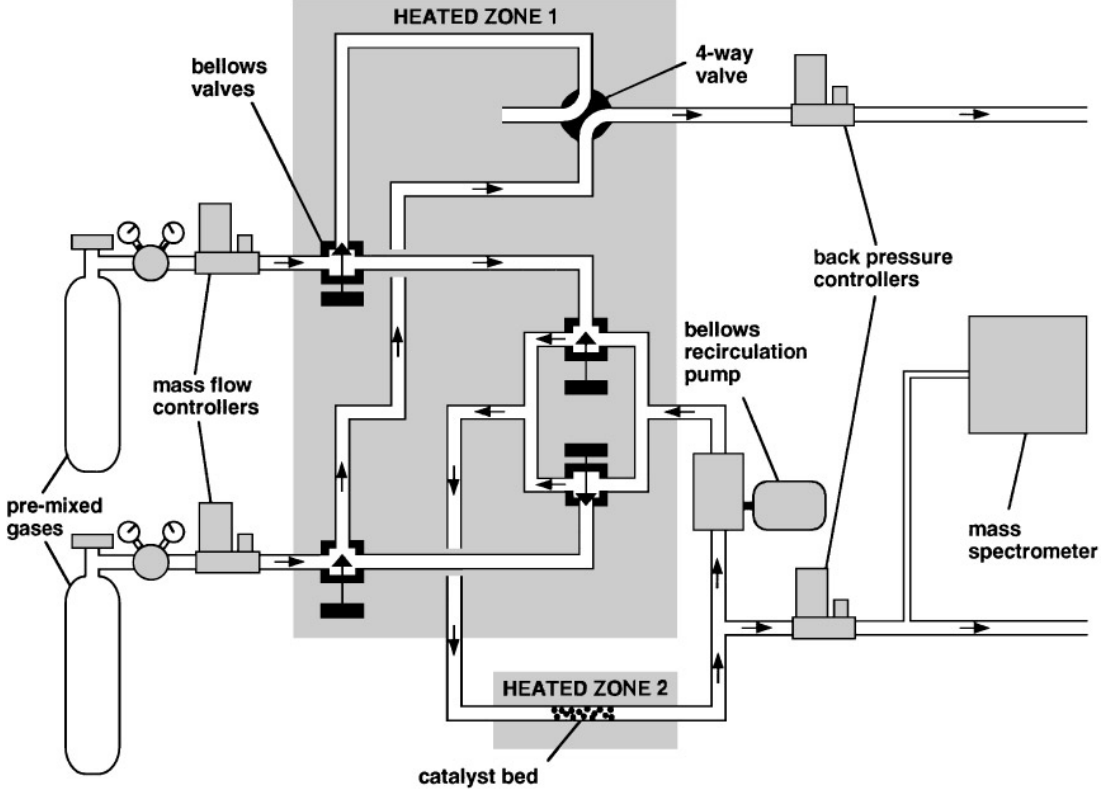

FIG. 1. Schematic diagram of experimental apparatus.

(NTP) and the pressure in the reactor was set at 1.3 bar. Before each run, the catalyst was reduced in flowing H_2 (50 ml/min NTP) at 450°C for 10 h.

A recirculating reactor system rather than a single-pass reactor was used because a homogeneous gas phase was desired. That simplified the computer simulation of the results and the extraction of rate constants from the data. Where possible, the recirculating system was constructed of glass-lined stainless steel tubing. That included the catalyst zone, which consisted of a removable U-shaped glass-lined stainless steel tube in which 200 mg of catalyst were held between wads of quartz wool. This tube had an inner diameter of 2.5 mm, which gave a catalyst bed height of 18 mm. The only parts of the recirculating system that were not glass-lined were two stainless steel metal gasket fittings that permitted the removal of the reactor zone, the four stainless steel bellows valves that controlled the flow into the system, and a stainless steel bellows recirculation pump. This pump delivered a recirculation flow rate of about 10 l/min (NTP), sufficient to maintain well-mixed conditions. With the exception of the bellows pump, the recirculating system could be heated, the reactor zone with its own oven, and the rest with a heated box covering the tubing and the valves.

Computer Simulations

To extract rate constants from the experimental data, the results were fitted to computer models with the program CATALYST II (30). One module of this program accepts as input a series of elementary reactions, their rate constants, and a description of transient reaction conditions and proceeds to calculate gas-phase and surface concentrations as a function of time by solving the mass balances of all reactants, products, and surface intermediates. It can also adjust rate constants to fit the calculated results to experimental data. Another module, which simulates a plug flow reactor operating at steady state and can also adjust rate constants to fit calculated results to experiments, was used to construct the overall microkinetic model.

RESULTS

Reaction of CD_4 with H_2

The reaction of deuterated methane with hydrogen was found to begin over our nickel catalyst at a temperature of about 350°C. We studied the reaction in the region from 350 to 450°C. Figure 2 shows concentrations of different types of methane observed in the effluent at 425°C before and after switches between 5% CH_4/H_2 and 5% CD_4/H_2. Figure 3 shows steady-state effluent concentrations of the different types of methane at various temperatures, obtained 15 min after each switch from 5% CH_4/H_2 to 5% CD_4/H_2. At low temperatures, the dominant product is CD_3H, in which only one of the deuterium atoms in CD_4 has

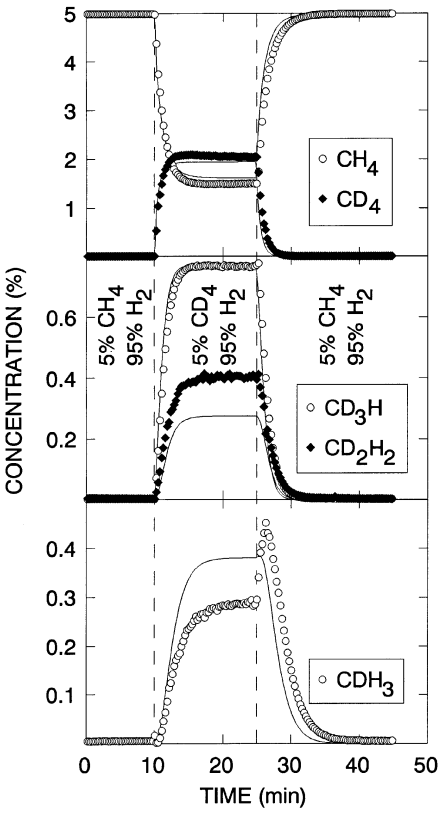

FIG. 2. Transient responses measured during reaction of CD_4 with H_2 at 425°C. Catalyst weight: 200 mg. Flow rate: 50 ml/min NTP. Pressure: 1.3 bar. Markers are experimental data, solid lines are microkinetic model.

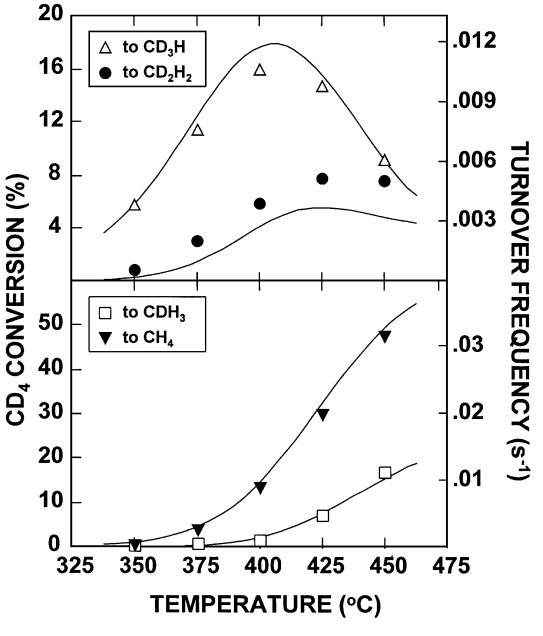

FIG. 3. Steady-state conversions of CD_4 to different products as a function of temperature. Catalyst weight: 200 mg. Flow rate: 50 ml/min NTP. Pressure: 1.3 bar. Markers are experimental data, solid lines are microkinetic model.

been exchanged with H. As the temperature is raised, however, the concentration of this product goes through a maximum and the dominant product becomes CH_4, in which all the deuterium atoms have been exchanged with H.

The observed steady-state concentrations versus temperature for all four methane products and the concentrations versus time obtained at each temperature could be satisfactorily described by the following microkinetic model, which assumes mass action kinetics, ignores kinetic isotope effects, and expresses each rate constant as the product of a preexponential factor times an exponential term containing an activation energy:

1. $CX_4 + 2* \leftrightarrow *CX_3 + *X$

$$k_{+1} = \frac{1.55 \times 10^7 \text{ molec.}}{\text{bar} \cdot \text{site} \cdot \text{s}} \exp\left(\frac{-53.4 \text{ kJ/mol}}{RT}\right)$$

$$k_{-1} = \frac{2.50 \times 10^{10} \text{ molec.}}{\text{site} \cdot \text{s}} \exp\left(\frac{-95.9 \text{ kJ/mol}}{RT}\right)$$

2. $*CX_3 + * \leftrightarrow *CX_2 + *X$

$$k_{+2} = \frac{1.00 \times 10^{13} \text{ molec.}}{\text{site} \cdot \text{s}} \exp\left(\frac{-115.4 \text{ kJ/mol}}{RT}\right)$$

$$k_{-2} = \frac{2.00 \times 10^{12} \text{ molec.}}{\text{site} \cdot \text{s}} \exp\left(\frac{-75.4 \text{ kJ/mol}}{RT}\right)$$

3. $*CX_2 + * \leftrightarrow *CX + *X$

fast

4. $2*X \leftrightarrow X_2 + 2*$

$$k_{+4} = \frac{1.00 \times 10^{13} \text{ molec.}}{\text{site} \cdot \text{s}} \exp\left(\frac{-95.0 \text{ kJ/mol}}{RT}\right)$$

$$k_{-4} = \frac{3.00 \times 10^{8} \text{ molec.}}{\text{bar} \cdot \text{site} \cdot \text{s}}.$$

In the above representation, X is either H or D; k_{+n}, k_{-n} are rate constants in the forward and reverse direction; $*$ is a nickel site; R is the gas constant; and T is the absolute temperature. The number of significant figures reflects the model's sensitivity and not the accuracy of the fit. The absence of an elementary reaction leading to adsorbed carbon in the scheme, such as $*CX + * \leftrightarrow *C + *X$, does not imply the absence of such a reaction in the actual mechanism but rather how its kinetics are inconsequential to the results of the model. The neglect of kinetic isotope effects can be justified by recent CH_4 and CD_4 dry reforming results obtained over Ni/SiO_2, in which rates of reaction were found to differ by only about 25% for the two isotopes (31). However, it should be pointed out that very different kinetic isotope effects have been observed for different Ni crystallographic planes during CH_4 and CD_4 decomposition experiments conducted over single crystals (32).

Five parameters were adjusted to fit the model to the experimental data. They were the four parameters describing the rate constants of reaction 1 in both the forward and the reverse directions and the forward activation energy of reaction 2. All the other parameters were estimated a priori. The forward preexponential factor of reaction 2 was assumed to be 10^{13} s^{-1}, which is the order of magnitude of k_BT/h (k_B = the Boltzmann constant, h = Planck's constant) and would be the value expected from transition state theory if the reaction's transition state and $^*{-}CX_3$ had similar partition functions. The parameters for the reverse rate constant of reaction 2 were adjusted later in the study by fitting other data, as the above model was found to be insensitive to their values. The forward preexponential factor of reaction 4 was also assumed to be 10^{13} s^{-1}, a value justified by transition state theory if the transition state and a pair of adsorbed hydrogen atoms have similar partition functions. The forward activation energy of reaction 4 was assumed to be the enthalpy change measured for this reaction over Ni(100) (33). The reverse preexponential factor for Step 4 was calculated by assuming a hydrogen sticking coefficient of 0.4 at a temperature of 350°C. Initial hydrogen sticking coefficients between 0.1 and 0.7 have been measured for Ni(100) at gas temperatures between 100 and 700°C or the equivalent molecular beam normal kinetic energy (34–38). The reverse activation energy of reaction 4 was assumed to be zero, an assumption corresponding to nonactivated adsorption.

Also shown in Figs. 2 and 3 are predictions obtained with the above model. Although the experiments and the model are for the most part in agreement, the place where they diverge the most is the peak obtained in the CDH_3 concentration after switching back from 5% CD_4/H_2 to 5% CH_4/H_2. According to the model, that peak arises because during the experiment the hydrogen coverage is much higher than the methyl coverage. After the switch, the surface $*CH_3$ coverage rises to its final value faster than the $*D$ coverage drops to its final value. The CDH_3 concentration, being roughly proportional to the product of these coverages, first rises because of the rise in the $*CH_3$ coverage and later drops because of the drop in the $*D$ coverage. Both the experimental data and the calculations contain the peak, but the model underestimates its width and height. The magnitude of that peak is primarily determined by the rate at which the $*D$ coverage drops after switch. That rate depends on the rate constants of reaction 4, which were not varied in the model to fit the data but rather estimated from the surface science literature. The most likely cause for the disagreement is the fact that the model ignores kinetic isotope effects, and $*D$ probably desorbs slower than $*H$. Kinetic isotope effects could not be included in the model without introducing too many adjustable parameters.

TABLE 1

Comparison of Model Parameters for Methane Adsorption and Dehydrogenation with Previously Published Values

Parameter	Ni/$MgAl_2O_4$–MgO (this work)	Ni(100) (molec. beam expts.)	Ni(111) (quantum mech. calc.)	Reference
CH_4 sticking coefficient at 400 K	4.4×10^{-9}	1.5×10^{-9}		39
		1.7×10^{-9}		40
CH_4 adsorption activation energy (kJ/mol)	54	52		39
		59		40
Ni–CH_3 bond strength (kJ/mol)	204		205	41
			179	42

Some of the parameters derived from fitting the data of Figs. 2 and 3 can be compared with literature values. This is done in Table 1. For example, Chorkendorff *et al.* measured methane sticking coefficients as a function of temperature over a Ni(100) surface using molecular beam techniques (39, 40). The groups of Siegbahn and Panas and Burghgraef *et al.* calculated Ni–CH_3 bond strengths for a Ni(111) surface using ab initio quantum mechanical methods (41, 42). The agreement between the values obtained by fitting the transient response curves and the literature results is encouraging, especially considering how they were obtained through very different methods.

Reaction of H_2O with D_2

The reaction of water with deuterium was found to begin over our nickel catalyst at a relatively low temperature (<100°C). We studied the temperature region between 100 and 200°C. In this range, we found that the reaction could proceed over the catalyst but not over a blank support. Figure 4 shows concentrations of different types of water observed in the reactor effluent at 150°C before and after switches between 100% H_2 and 3.3% H_2O/D_2. Figure 5 shows steady-state effluent concentrations of the different types of water at various temperatures, obtained 25 min after the switch from 100% H_2 and 3.3% H_2O/D_2. In this case, the transient results obtained at a given temperature present more features than steady-state results at various temperatures. Right after the switch from hydrogen to the H_2O/D_2 mixture, an immediate rise is seen in the H_2O concentration as water is allowed into the recirculating system. However, as water begins to react with the Ni surface and desorb as HDO and D_2O, the H_2O concentration begins to fall. Because the hydrogen on the Ni surface is initially mainly H, the first product that appears is HDO. However, gradually most of the hydrogen on the Ni surface becomes D, the HDO concentration falls, and the D_2O concentration increases.

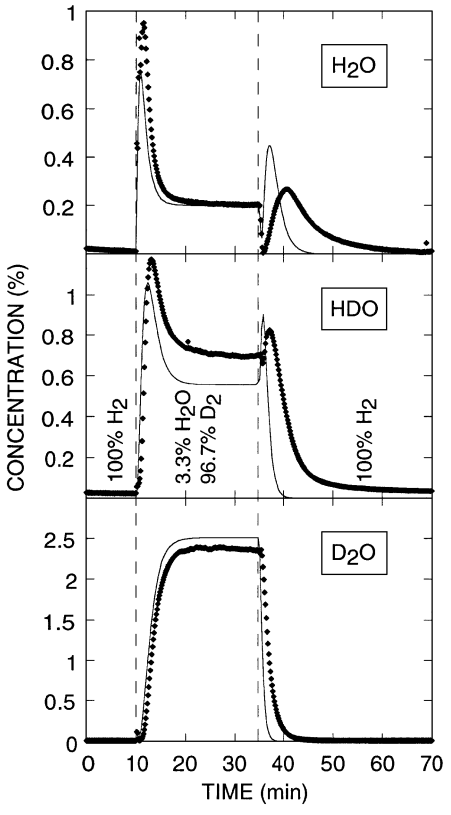

FIG. 4. Transient responses measured during reaction of H_2O with D_2 at 150°C. Catalyst weight: 200 mg. Flow rate: 50 ml/min NTP. Pressure: 1.3 bar. Markers are experimental data, solid lines are microkinetic model.

The observed transient concentrations at each temperature and the steady-state concentrations versus temperature could be satisfactorily described by the following microkinetic model, which involves the same kind of assumptions and is presented in the same manner as that of

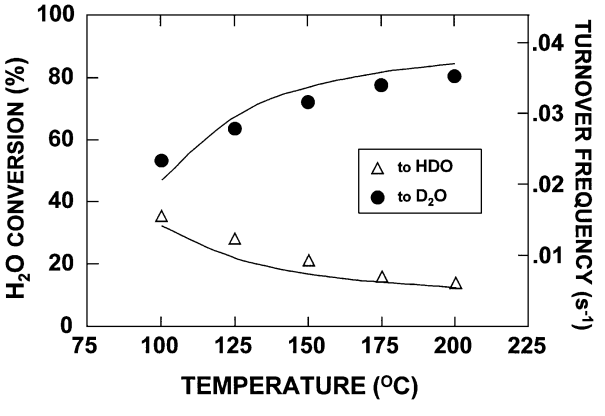

FIG. 5. Steady-state conversions of H_2O to different products as a function of temperature. Catalyst weight: 200 mg. Flow rate: 50 ml/min NTP. Pressure: 1.3 bar. Markers are experimental data, solid lines are microkinetic model.

the previous section (once again, $X = \mathrm{H}$ or D):

1. $X_2\mathrm{O} + * \leftrightarrow *X_2\mathrm{O}$

$$k_{+1} = \frac{1.78 \times 10^6 \text{ molec.}}{\text{bar} \cdot \text{site} \cdot \text{s}}$$

$$k_{-1} = \frac{1.00 \times 10^{13} \text{ molec.}}{\text{site} \cdot \text{s}} \exp\left(\frac{-64.4 \text{ kJ/mol}}{RT}\right)$$

2. $*X_2\mathrm{O} + * \leftrightarrow *\mathrm{O}X + *X$

$$k_{+2} = \frac{4.15 \times 10^7 \text{ molec.}}{\text{site} \cdot \text{s}}$$

$$k_{-2} = \frac{3.08 \times 10^{11} \text{ molec.}}{\text{site} \cdot \text{s}} \exp\left(\frac{-32.2 \text{ kJ/mol}}{RT}\right)$$

3. $2*X \leftrightarrow X_2 + 2*$

$$k_{+3} = \frac{1.00 \times 10^{13} \text{ molec.}}{\text{site} \cdot \text{s}} \exp\left(\frac{-95.0 \text{ kJ/mol}}{RT}\right)$$

$$k_{-3} = \frac{3.00 \times 10^8 \text{ molec.}}{\text{bar} \cdot \text{site} \cdot \text{s}}$$

It should be noted that agreement between the model and the experimental data could only be obtained when elementary reactions leading to complete water dissociation, such as $*\mathrm{O}X + * \leftrightarrow *\mathrm{O} + *X$, were excluded from the model. This implies that complete dissociation was not occurring in the studied temperature region; however, that does not preclude it from occurring at higher temperatures.

Three parameters were adjusted to fit the model to the experimental data. They were the forward temperature-independent rate constants of reactions 1 and 2 and the reverse activation energy of reaction 1. The reverse preexponential factor of reaction 1 was assumed to be $k_B T/h$, or 10^{13} s^{-1}, a value justified by transition state theory if the transition state and adsorbed molecular water have similar partition functions. The parameters for the reverse rate constant of reaction 2 were adjusted later in the study by fitting other data, as the above model was found to be insensitive to their values. Reaction 3 in the above model is the same as reaction 4 of the previous section, and its parameters were estimated as described in that section.

Also shown in Figs. 4 and 5 are predictions obtained with the model. These predictions agree with the experimental data obtained right after the switch from 100% H_2 to 3% H_2O/D_2 is made. However, when a switch is later made from 3% H_2O/D_2 back to 100% H_2, the model and experiments agree qualitatively but not quantitatively. The model predicts changes that are faster than what is observed experimentally. This discrepancy is attributed to adsorption of HDO and D_2O on the support and on the stainless steel parts of the recirculating system, which retards the rate at which deuterium is flushed out of the system. Because the model only considers water adsorption on the nickel surface, it predicts faster changes.

The model considered water adsorption only on the nickel surface because the experiments conducted over a blank support showed that water dissociation could not occur in the absence of nickel in the studied temperature regime. That does not mean that water dissociation cannot occur on the support at higher temperatures, nor does it rule out molecular adsorption of water on the support and the spillover of molecular water between the support and the nickel surface. However, molecular water adsorption on the support does little more than broaden the features of curves such as that shown in Fig. 4. The features observed after the switch to 3% H_2O/D_2 are not affected as much because at that stage the net rate of adsorption onto the support (adsorption minus desorption) is small compared to the rate at which water is fed into the reactor and because the deuterium content of the water desorbing from the support lies somewhere between that of the feed and that of the gas phase. The features observed after the switch back to 100% H_2 are affected to a larger extent because at that stage desorption from the support is the major source of new water coming into the gas phase and because the deuterium content of this water is considerably higher than that of the water already in the gas phase. The spillover of molecular water probably affects the parameters of the first reaction in the model; however, the measured parameters can still be of use as effective parameters combining water adsorption directly from the gas phase and via spillover from the support.

Transient CO Methanation

Figure 6 shows effluent CH_4 concentrations measured during CO methanation experiments involving switches between 100% H_2 and CO/H_2 mixtures. Carbon monoxide adsorbs rather strongly on nickel; thus, it is possible to find CO methanation conditions under which the surface is nearly completely covered with CO. When this happens, the reaction rate is limited by the availability of sites onto which hydrogen can adsorb, and the reaction exhibits a negative reaction order with respect to CO. If one switches from 100% H_2 to such a set of conditions, the methane production initially rises but later drops after the CO concentration has reached the point where the CO coverage starts approaching unity (Fig. 6a). If the temperature is too high or the CO concentration in the CO/H_2 mixture is too low, the CO coverage cannot reach values approaching unity and the effect is not as pronounced (Fig. 6b).

Experiments of this type have been reported before over Ni and Rh catalysts (43–46). In one study over a Rh catalysts (45), catalyst coking was reported to occur along with methanation. That was not the case in our work because our CO partial pressures were lower and because our Ni catalyst was based on a more coke-resistant support. We know this to be the case because, as observed in a previous study performed under conditions similar to ours (43), the

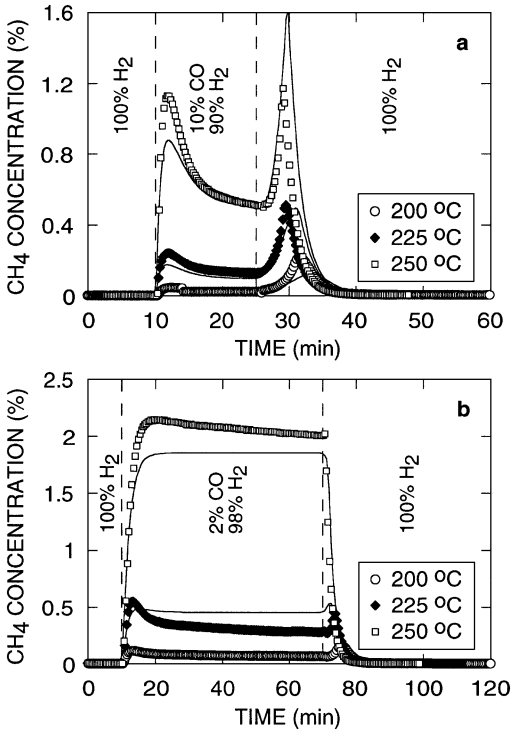

FIG. 6. Transient CH_4 responses measured during reaction of CO with H_2. Catalyst weight: 200 mg. Flow rate: 50 ml/min NTP. Pressure: 1.3 bar. Markers are experimental data, solid lines are microkinetic model.

amount of water produced during reaction corresponded to the amount of methane, although the water curves were noisier and a little broader than the methane curves shown in Fig. 6. If there would have been coking, more methane than water would have been produced right after the step back to 100% H_2.

The experimental curves of Fig. 6 could be explained by the following microkinetic model, whose predictions are shown along with the experimental data:

1. $H_2 + 2* \leftrightarrow 2*H$

$$k_{+1} = \frac{3.00 \times 10^8 \text{ molec.}}{\text{bar} \cdot \text{site} \cdot \text{s}}$$

$$k_{-1} = \frac{1.00 \times 10^{13} \text{ molec.}}{\text{site} \cdot \text{s}} \exp\left(\frac{-95.0 \text{ kJ/mol}}{RT}\right)$$

2. $CO + 2* \leftrightarrow **CO$

$$k_{+2} = \frac{1.00 \times 10^8 \text{ molec.}}{\text{bar} \cdot \text{site} \cdot \text{s}}$$

$$k_{-2} = \frac{5.00 \times 10^{12} \text{ molec.}}{\text{site} \cdot \text{s}} \exp\left(\frac{-115.0 \text{ kJ/mol}}{RT}\right)$$

3. $*H + **CO + 2* \rightarrow **CHO + 3*$

$$k_{+3} = \frac{1.00 \times 10^7 \text{ molec.}}{\text{site} \cdot \text{s}} \exp\left(\frac{-23.0 \text{ kJ/mol}}{RT}\right)$$

4. $**CHO + 5*H \rightarrow CH_4 + H_2O + 7*$

fast.

Two parameters were adjusted in the model to fit the experimental data. They were the preexponential factor and the activation energy of reaction 3. Reaction 1 appears in the models described in the previous two sections and the estimates for its rate constants have been explained above. The forward temperature-independent rate constant of reaction 2 is an assumption corresponding to a CO sticking coefficient of 0.5 at a temperature of 350°C. An initial sticking coefficient between 0.6 and 0.9 has been measured over Ni(100); however, this sticking coefficients drops to less than half its original value as the coverage is increased from 0 to 0.5 monolayers (47–49). The reverse preexponential factor of reaction 2 was assumed to be $\frac{1}{2}k_B T/h$, a value justified by transition state theory if the transition state and adsorbed CO have similar partition functions (the factor of $\frac{1}{2}$ arises because a coverage of unity corresponds to one molecule of CO for every two surface Ni sites). The reverse activation energy of reaction 2 was assumed to be minus its enthalpy change, which was measured by calorimetry to be between 105 and 125 kJ/mol at coverage from 0 to 0.4 monolayers on Ni(100) (47). Adsorbed CO was assumed to occupy two Ni sites in the model because at higher than 0.5 monolayers both the CO sticking coefficient and the adsorption energy drop significantly over Ni(100) (47) and because LEED studies over Ni(100) have identified a $c(2 \times 2)$ structure that exists only up to 0.5 monolayers (50). Reaction 4 is not an elementary reaction but rather a series of fast reactions whose kinetics are irrelevant because they come after the rate-determining step.

The key to the above model is reaction 3, the rate-determining step, an elementary reaction requiring an ensemble of five Ni sites. There is, to our knowledge, no previous evidence of such a reaction in the literature. We are likewise unaware of any previously reported evidence that would point to structure sensitivity in the CO methanation reaction, which the five-site ensemble could suggest. However, without that assumption the experimental data could not be simulated while with the assumption all curves could be explained by adjusting only two parameters.

Overall Microkinetic Model

The experimental results described in the previous three sections present a partial microkinetic picture of methane reforming. To complete the picture, we constructed an overall microkinetic model, filling in gaps and adjusting unknown rate constants until the overall model could explain the steady-state kinetics of the reactions of methane with steam and carbon dioxide with hydrogen. The experimental data used for adjusting the overall model were

those reported by Xu and Froment (51, 52), who measured the intrinsic kinetics of these reactions over a nickel catalyst based on a $MgAl_2O_4$ support. When methane was reacted with steam under Xu and Froment's conditions, the steam reforming reaction and the water–gas shift reaction ($CO + H_2O \rightarrow CO_2 + H_2$) both occurred. Likewise, when carbon dioxide was reacted with hydrogen, the reverse water–gas shift reaction and CO_2 methanation both occurred. These authors actually constructed a model based on the Langmuir–Hinshelwood approach to explain their data. We constructed a different model, based on a microkinetic approach and on the results of the previous sections, to explain the same data. Figures 7 and 8 show how our overall microkinetic was able to simulate the results measured by these investigators as they varied temperature and contact time. The model was also able to simulate the trends observed when the total pressure and the ratios of reactants were varied, although those results are not shown here for reasons of brevity (a total of 88 curves were measured by Xu and Froment and used to adjust the model). The overall microkinetic we constructed consisted of the following thirteen reactions:

1. $CH_4 + 2* \leftrightarrow *CH_3 + *H$

$$k_{+1} = \frac{1.55 \times 10^7 \text{ molec.}}{\text{bar} \cdot \text{site} \cdot \text{s}} \exp\left(\frac{-53.9 \text{ kJ/mol}}{RT}\right)$$

$$k_{-1} = \frac{2.50 \times 10^{10} \text{ molec.}}{\text{site} \cdot \text{s}} \exp\left(\frac{-95.9 \text{ kJ/mol}}{RT}\right)$$

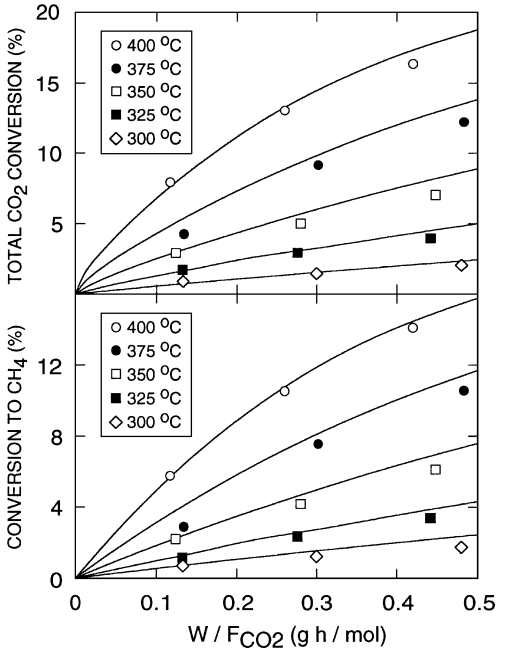

FIG. 7. Comparison of microkinetic model with previously published data for CO_2 methanation. Markers are experimental data from Refs. (51, 52), solid lines are microkinetic model.

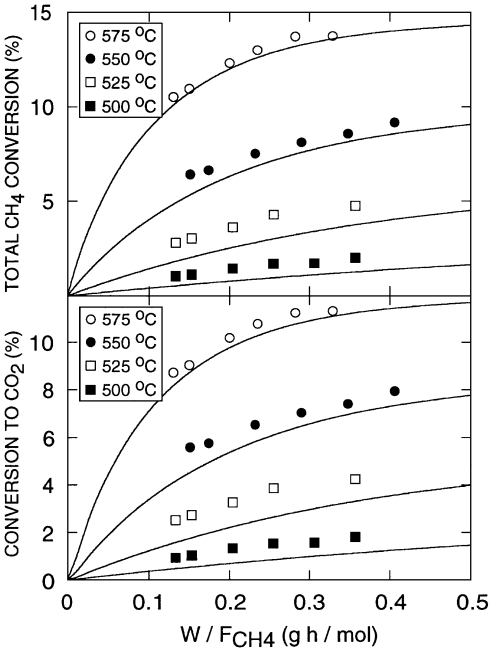

FIG. 8. Comparison of microkinetic model with previously published data for low-temperature methane reforming with steam. Markers are experimental data from Refs. (51, 52), solid lines are microkinetic model.

2. $*CH_3 + * \leftrightarrow *CH_2 + *H$

$$k_{+2} = \frac{1.00 \times 10^{13} \text{ molec.}}{\text{site} \cdot \text{s}} \exp\left(\frac{-115.4 \text{ kJ/mol}}{RT}\right)$$

$$k_{-2} = \frac{2.00 \times 10^{12} \text{ molec.}}{\text{site} \cdot \text{s}} \exp\left(\frac{-75.4 \text{ kJ/mol}}{RT}\right)$$

3. $*CH_2 + * \leftrightarrow *CH + *H$

$$k_{+3} = \frac{1.00 \times 10^{13} \text{ molec.}}{\text{site} \cdot \text{s}} \exp\left(\frac{-102.9 \text{ kJ/mol}}{RT}\right)$$

$$k_{-3} = \frac{2.00 \times 10^{12} \text{ molec.}}{\text{site} \cdot \text{s}} \exp\left(\frac{-84.7 \text{ kJ/mol}}{RT}\right)$$

4. $*CH + * \leftrightarrow *C + *H$

$$k_{+4} = \frac{1.00 \times 10^{13} \text{ molec.}}{\text{site} \cdot \text{s}}$$

$$k_{-4} = \frac{2.00 \times 10^{12} \text{ molec.}}{\text{site} \cdot \text{s}} \exp\left(\frac{-64.4 \text{ kJ/mol}}{RT}\right)$$

5. $H_2O + * \leftrightarrow *H_2O$

$$k_{+5} = \frac{1.78 \times 10^6 \text{ molec.}}{\text{bar} \cdot \text{site} \cdot \text{s}}$$

$$k_{-5} = \frac{1.00 \times 10^{13} \text{ molec.}}{\text{site} \cdot \text{s}} \exp\left(\frac{-64.4 \text{ kJ/mol}}{RT}\right)$$

6. $*H_2O + * \leftrightarrow *OH + *H$

$$k_{+6} = \frac{4.15 \times 10^7 \text{ molec.}}{\text{site} \cdot \text{s}}$$

$$k_{-6} = \frac{3.08 \times 10^{11} \text{ molec.}}{\text{site} \cdot \text{s}} \exp\left(\frac{-32.2 \text{ kJ/mol}}{RT}\right)$$

7. $*C + *OH \leftrightarrow **CHO$

$$k_{+7} = \frac{1.00 \times 10^{13} \text{ molec.}}{\text{site} \cdot \text{s}} \exp\left(\frac{-65.5 \text{ kJ/mol}}{RT}\right)$$

$$k_{-7} = \frac{2.12 \times 10^{19} \text{ molec.}}{\text{site} \cdot \text{s}} \left(\frac{1}{T}\right)^{3.033} \exp\left(\frac{-90.3 \text{ kJ/mol}}{RT}\right)$$

8. $CO_2 + 2* \leftrightarrow **CO_2$

in equilibrium

9. $**CO_2 + *H \leftrightarrow **COOH + *$

in equilibrium

10. $**COOH + *H + 2* \leftrightarrow * * CHO + *OH + 2*$

$$K_8 K_9 k_{+10} = \frac{34,400 \text{ molec.}}{\text{bar} \cdot \text{site} \cdot \text{s}} \left(\frac{1}{T}\right)^{.968} \exp\left(\frac{+50.0 \text{ kJ/mol}}{RT}\right)$$

$$k_{-10} = \frac{1.00 \times 10^{13} \text{ molec.}}{\text{site} \cdot \text{s}}$$

11. $**CHO + 3* \leftrightarrow **CO + *H + 2*$

$$k_{+11} = \frac{5.14 \times 10^9 \text{ molec.}}{\text{site} \cdot \text{s}}$$

$$k_{-11} = \frac{1.00 \times 10^7 \text{ molec.}}{\text{site} \cdot \text{s}} \exp\left(\frac{-23.0 \text{ kJ/mol}}{RT}\right)$$

12. $**CO \leftrightarrow CO + 2*$

$$k_{+12} = \frac{5.00 \times 10^{12} \text{ molec.}}{\text{site} \cdot \text{s}} \exp\left(\frac{-115.0 \text{ kJ/mol}}{RT}\right)$$

$$k_{-12} = \frac{1.00 \times 10^8 \text{ molec.}}{\text{bar} \cdot \text{site} \cdot \text{s}}$$

13. $2*H \leftrightarrow H_2 + 2*$

$$k_{+13} = \frac{1.00 \times 10^{13} \text{ molec.}}{\text{site} \cdot \text{s}} \exp\left(\frac{-95.0 \text{ kJ/mol}}{RT}\right)$$

$$k_{-13} = \frac{3.00 \times 10^8 \text{ molec.}}{\text{bar} \cdot \text{site} \cdot \text{s}}$$

In addition to the reactions used to simulate the experiments of the previous sections, this model has reactions describing the dehydrogenation of $*CH_2$ to a surface carbidic carbon ($*C$, reactions 3 and 4), the reaction of surface carbon and surface hydroxyls to form $**CHO$ (reaction 7), and the formation of $**CHO$ from carbon dioxide through a surface formate intermediate (reactions 8–10). Reactions 3, 4, and 7 describe in the simplest way possible those parts of the mechanism denoted as "fast" in the previous sections. Reactions 8–10 are necessary to describe reactions involving CO_2. Justification for a surface formate intermediate in these steps can be found in the literature. For example, formate species on nickel surfaces are stable enough that they have been characterized by both HREELS and RAIRS (53–55). The existence of a mechanism linking such a formate species with CO, CO_2 and H_2 has been demonstrated by flash desorption of formic acid from nickel surfaces (56). Surface formate species have also been implicated as intermediates in methanol synthesis, whose reaction pathway shares several surface reactions with the pathways of reactions described here (57). A five-site ensemble for reaction 10 was chosen because such an ensemble was found to best describe Xu and Froment's data. In the model, all surface species containing both carbon and oxygen were assumed to occupy two Ni sites. The justification for surface CO was given in the previous section. The justification for surface formate can be found in HREELS and RAIRS experiments (53–55). The assumption for the other two species, $**CHO$ and $**CO_2$, was made by inference and was not important, as these species are predicted to have very low coverages over the entire range of conditions.

The model presented above is by no means unique. Similar models could have been developed with complete water dissociation to $*O$ or dissociation of $**CO_2$ to $**CO$ and $*O$. However, such models would have involved extra reactions and extra adjustable parameters. One could also argue that although a surface formate species is justified by low temperature experiments, its presence at higher temperatures is not guaranteed. The absence of $*O$ and the presence of $**COOH$ in our model reflect simplicity rather than any ability of microkinetic modeling to discriminate whether such species are involved in the actual mechanism.

Eight parameters were adjusted in the model to fit the experimental data. The first seven were the forward preexponential factor of reaction 11, the forward activation energies of reactions 3 and 7, the reverse preexponential factors of reactions 2 and 6, and the reverse activation energies of reactions 4 and 6. The eighth parameter was an adjustment factor by which all rates were uniformly decreased for the simulation of the steam reforming experiments. This was done because Xu and Froment observed some catalyst deactivation during steam reforming and measured all rates after the catalyst had deactivated to a certain determined amount (51, 52). The fitting procedure gave a nickel surface loss of 15% in these experiments. All other parameters were either taken from the experiments described above or estimated. The reverse activation energies of reactions 2 and 3 were estimated assuming Ni–CH_2 and Ni–CH bond energies given in Ref. (42). The preexponential factors of reactions 3 and 4 were assumed to be equal to those of reaction 2. The forward preexponential factor of reaction 7 and the reverse preexponential of reaction 10 were assumed to

TABLE 2

Comparison of Microkinetic Model Predictions for CO Methanation with Previously Published Data (Ref. 58)

Quantity	Ni/Al_2O_3	Model
Turnover frequency (s^{-1})	2.7×10^{-2} to 1.1×10^{-1}	6.6×10^{-3}
Activation energy (kJ/mol)	109 to 138	124
H_2 reaction order	0.7 to 0.8	0.72
CO reaction order	−0.5 to −0.2	−0.63

be 10^{13} s^{-1}, justified by transition state theory. The reverse rate constant for reaction 7 and the forward rate constant of reaction 10 were set so the rate constants in the model would be consistent with the equilibrium constants of the steam reforming and water–gas shift reactions, whose equilibrium constants versus temperature (1) were fit to the empirical equations

$$CH_4 + H_2O \leftrightarrow CO + 3H_2$$

$$K_{eq} = 810(T)^{3.03} \exp\left(\frac{-202.3\ \text{kJ/mol}}{RT}\right)$$

$$CO + H_2O \leftrightarrow CO_2 + H_2$$

$$K_{eq} = 9.01 \times 10^{-6}(T)^{0.968} \exp\left(\frac{43.6\ \text{kJ/mol}}{RT}\right)$$

Table 3 summarizes the origin of each parameter in the overall model.

By adjusting the 8 parameters mentioned above, the model was able to satisfactorily simulate all 88 curves measured by Xu and Froment for steam reforming and the reaction of CO_2 with hydrogen over a nickel catalyst. In theory, the model should describe several reactions, including methane reforming with both steam and CO_2, CO, and CO_2 methanation and the water–gas shift reaction. A more stringent test of the model is therefore to compare its predictions with data that was not used for the adjustment of parameters. One such test is shown in Table 2, where predictions of the model are compared with data published for the kinetics of CO methanation over several Ni/Al_2O_3 catalysts (58). Although the model's prediction for the reaction rate under the conditions of that study is about an order of magnitude too low, all the major trends are correctly predicted.

Another example is shown in Fig. 9, where the model's prediction are compared with published experimental data for CO methanation over a nickel single crystal (59). This time the model had to be modified to simulate the data. Since the experiments in Fig. 9 were collected with a substantially higher CO/H_2 ratio in the feed than those shown in Table 2, they lead to higher coverages of carbon on the catalyst. The unmodified model predicted very high

TABLE 3

Origins of Rate Constants in Overall Microkinetic Model

Reaction	Forward prexep. factor	Forward activation energy	Reverse prexep. factor	Reverse activation energy
1	$CD_4 + H_2$ experiment	$CD_4 + H_2$ experiment	$CD_4 + H_2$ experiment	$CD_4 + H_2$ experiment
2	Assumption based on transition state theory	$CD_4 + H_2$ experiment	Fitting of data from Refs. (51, 52)	Assumption based on literature (Ref. 41)
3	Assumption based on similarity between reactions 2–4	Fitting of data from Refs. (51, 52)	Assumption based on similarity between reactions 2–4	Assumption based on literature (Ref. 41)
4	Assumption based on similarity between reactions 2–4	0	Assumption based on similarity between reactions 2–4	Fitting of data from Refs. (51, 52)
5	$H_2O + D_2$ experiment	0	Assumption based on transition state theory	$H_2O + D_2$ experiment
6	$H_2O + D_2$ experiment	$H_2O + D_2$ experiment	Fitting of data from Refs. (51, 52)	Fitting of data from Refs. (51, 52)
7	Assumption based on transition state theory	Fitting of data from Refs. (51, 52)	Equil. constant, $CH_4 + H_2O \leftrightarrow CO + 3H_2$	Equil. constant, $CH_4 + H_2O \leftrightarrow CO + 3H_2$
8–10	Equil. constant, $CO + H_2O \leftrightarrow CO_2 + H_2$	Equil. constant, $CO + H_2O \leftrightarrow CO_2 + H_2$	Assumption based on transition state theory	0
11	Fitting of data from Refs. (51, 52)	0	Transient CO methanation experiment	Transient CO methanation experiment
12	Assumption based on transition state theory	Assumption based on literature (Ref. 47)	0	Assumption based on literature (Refs. 47–49)
13	Assumption based on transition state theory	Assumption based on literature (Ref. 33)	0	Assumption based on literature (Refs. 34–38)

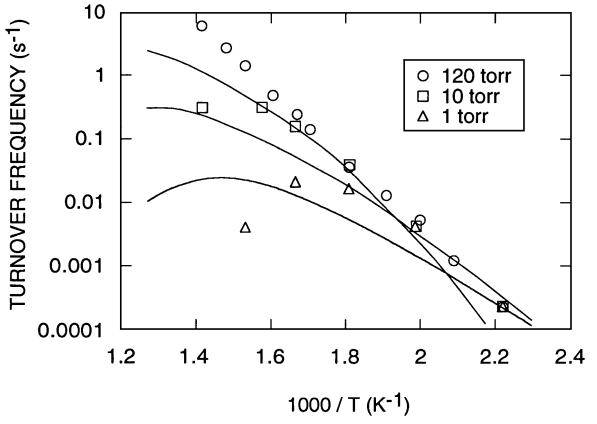

FIG. 9. Comparison of microkinetic model with previously published data for CO methanation over Ni(100). Markers are experimental data from Ref. (59), solid lines are microkinetic model.

surface carbide (∗C) coverages and thus very little reaction throughout almost the entire range of conditions shown in the figure. The modification required was one in which the ∗C coverage was forced to have a maximum of half a monolayer. It was with this modification that the curves shown in the figure were generated. Because the model predicted that the surface carbide assumed its maximum coverage throughout almost the entire range of conditions, this coverage was essentially constant at 0.5. In this fashion, the model is similar to that already published for the simulation of the same data, in which a constant carbon coverage was assumed (60). With the modification, the model can predict the major trends, although the predicted temperatures for a given behavior are about 100°C too high. The modification does not affect the calculation of curves shown in Figs. 7 and 8 nor the data of Table 2 because in those cases the calculated surface carbide concentration never reached a value as high as 0.5.

Figure 10 compares the modified model's predictions with published data for methane reforming with steam and carbon dioxide over a $Ni/MgO–MgAl_2O_4$ catalyst with a lower metal surface area than that used for the experiments of previous sections (10). The model actually overestimates the reaction rates under the conditions of that study, making direct comparison difficult. However, if the rates of all reactions in the model are multiplied by a factor of 0.2, one obtains the curves shown in the figure. Thus, although the model's rates are off by nearly an order of magnitude, it can nevertheless predict major trends such as activation energies and the fact that reforming with steam is faster than reforming with carbon dioxide.

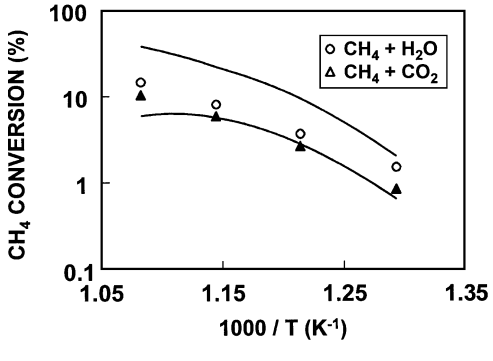

FIG. 10. Comparison of microkinetic model with previously published data for methane reforming with steam and CO_2. Markers are experimental data from Ref. (10), solid lines are microkinetic model with all rates multiplied times a factor of 0.2.

DISCUSSION

The kinetics of methane steam reforming have been studied by several investigators and summarized in previous reviews (1, 2, 61). Most rate expressions proposed to date have been found to be applicable only in a limited range of conditions. For example, Bodrov *et al.* assumed methane adsorption to be rate limiting and proposed the following expression based on experiments conducted over a nickel foil (62):

$$r = \frac{kP_{CH_4}}{1 + a\left(P_{H_2O}/P_{H_2}\right) + bP_{CO}}.$$

However, it has been observed that H_2 can retard the reaction under some conditions. That cannot be explained by the above expression.

Khomenko *et al.* (63) later proposed the following rate expression based on Temkin's general kinetic identity and a proposed reaction pathway

$$r = \frac{kP_{CH_4}P_{H_2O}\left(1 - \left(P_{CO}\left(P_{H_2}\right)^3/K_{eq}P_{CH_4}P_{H_2O}\right)\right)}{f\left(P_{H_2O}, P_{H_2}\right)\left(1 + \left(K_{H_2O}P_{H_2O}/P_{H_2}\right)\right)},$$

where K_{eq} is the equilibrium constant for the overall reaction and $f(P_{H_2O}, P_{H_2})$ is a polynomial in P_{H_2O} and P_{H_2}. However, when this expression was tested at high pressure over a nickel foil, the rate constant was found to be a function of the pressure.

Xu and Froment (52) have proposed three different Langmuir–Hinshelwood expressions for the following three reactions, all of which occur simultaneously through separate pathways under steam reforming and methanation conditions:

$$CH_4 + H_2O \rightarrow CO + 3H_2$$

$$CO + H_2O \rightarrow CO_2 + H_2$$

$$CH_4 + 2H_2O \rightarrow CO_2 + 4H_2.$$

Their proposed rate expression for the first reaction, the most important under typical steam reforming conditions,

was

$$r = \frac{\left(kP_{CH_4}P_{H_2O}/P_{H_2}^{2.5}\right)\left(1-\left(P_{CO}\left(P_{H_2}\right)^3/K_{eq}P_{CH_4}P_{H_2O}\right)\right)}{1+K_{CO}P_{CO}+K_{H_2}P_{H_2}+K_{CH_4}P_{CH_4}+\left(K_{H_2O}P_{H_2O}/P_{H_2}\right)}.$$

Xu and Froment's rate expressions describe very well the experimental rates they measured for steam reforming and the reaction of CO_2 with hydrogen. These are the same experimental data on which our model was based. However, as pointed out before (2, 10), they imply a negative heat of adsorption for steam and are unable to predict the decrease in rate observed experimentally when steam is replaced by carbon dioxide.

The limitations in the applicability of these rate expressions suggest that there is no single rate-determining step in the reforming of methane and that no simple analytical expression can be valid over a wide range of conditions. We have shown that a microkinetic model with many parameters obtained either from the surface science literature or from fitting the results of transient kinetics experiments can in contrast explain many major trends over a wide range of conditions. The model's predictions are not quantitative, as predicted rates can deviate by as much as an order of magnitude from experimental ones. However, the model can predict correct activation energies, reaction orders, and other trends for several reactions, including steam reforming, dry reforming, CO methanation, CO_2 methanation, and the water–gas shift reaction and its reverse.

It is normal for microkinetic models to predict activation energies and reaction orders better than actual reaction rates (30). More cannot be expected, given the assumptions involved. Such models assume mass action kinetics with Arrhenius expressions presumed to be valid over a wide range of conditions. They often do not take into account all possible reaction pathways. They generally ignore adsorbate–adsorbate interactions and how the working catalyst surface may be different under reaction conditions than during the experiments on which their parameters are based. Nonetheless, they allow the consolidation in a semi-quantitative fashion of experimental data and theoretical principles from very diverse sources. Their value lies not in the precise quantitative prediction of catalytic performance but rather in the contribution they can make to our understanding of reaction mechanisms.

The microkinetic model described above is a good example, providing a wealth of mechanistic information. For instance, the model predicts that the slowest steps in the mechanism are reactions 1–3, 7, 10, and 11. Although these reactions may not necessarily occur exactly as written above, the prediction suggests that surface reactions involved in methane adsorption and dehydrogenation, the formation of a C–O bond, and the formation of a OC–O bond can all be slow steps. Under some conditions, one of them can be the rate-determining step, but under most conditions a combination of them determines the rate. Interestingly, the model predicts that the rate of steam reforming at high temperatures (550–800°C) is largely dependent on the rate of reaction 7, the step in which a C–O bond is formed. That step is predicted to be slow, not because its rate constant is low, but because the coverage of ∗OH drops quickly with temperature. Microkinetic modeling cannot establish whether ∗OH is the actual oxygen-containing species involved in C–O bond formation. Although reaction 7 is written as involving ∗OH, an equivalent model could have been developed involving ∗O instead. But the general conclusion can be drawn that the availability of surface oxygen can play a key role in determining the reaction rate at high temperatures.

The coverage of an oxygen-containing species like ∗OH is determined in large part by the rate constants of reactions 5 and 6, which involve water adsorption and dissociation. Although reaction 5 is written as the direct adsorption of water from the gas phase onto nickel, it is known that water can first adsorb on the support and subsequently spill over onto the nickel surface (1). The forward and reverse rate constants of reaction 5, as determined by the reaction of H_2O with D_2, are therefore effective rate constants that combine the kinetics of water adsorption directly from the gas phase and via spillover from the support. The implication of this is that these rate constants could be support dependent, and since those rate constant determine the availability of oxygen-containing surface species and that affects the overall rate of reaction, the model in essence suggests that overall reaction rates may depend on the support under some conditions.

The model predicts that under some reforming conditions the dissociative adsorption of methane (reaction 1) is reversible. The results therefore cast doubt on the often quoted assumption that methane adsorption is the rate-determining step during steam reforming. This is not surprising, given that the rate constants for methane adsorption and dehydrogenation in the model were derived from the experiments summarized in Fig. 3. That figure shows how this reaction begins at a temperature as low as 350°C and how its rate increases very quickly with temperature. Even if one ignores the microkinetic model, these data show how improbable it is for methane adsorption to be the sole rate-determining step at high temperatures.

The model also predicts coverages of carbidic carbon (∗C) under a variety of reaction conditions. Such carbon could well be a precursor of the graphitic carbon that causes deactivation. Not surprisingly, higher ∗C coverages are predicted during dry reforming than during steam reforming. The model identifies which elementary steps are important in determining the coverage of the carbidic carbon. They are, as expected, reactions 4 and 7, those involving surface

carbon. As mentioned above, the rate of reaction 7 depends on the availability of surface oxygen, which depends on the rate constants of water adsorption and dissociation, which in turn are a function of the support. That is likely part of the explanation of why some supports lead to more coke resistant catalysts than others.

ACKNOWLEDGMENTS

The author thanks J. R. Rostrup-Nielsen and J.-H. Bak Hansen for stimulating discussions and S. Rokni and H. McDougall for their help in collecting the experimental data.

REFERENCES

1. Rostrup-Nielsen, J. R., *in* "Catalysis, Science and Technology" (J. R. Anderson and M. Boudart, Eds.), Vol. 5, p. 1. Springer-Verlag, Berlin, 1984.
2. Rostrup-Nielsen, J. R., *Catal. Today* **18**, 305 (1993).
3. Zhang, Z. L., Tsipourari, V. A., Efstathiou, A. M., and Verykios, X. E., *J. Catal.* **158**, 51 (1996).
4. Efstathiou, A. M., Kladi, A., Tsipourari, V. A., and Verykios, X. E., *J. Catal.* **158**, 64 (1996).
5. Erdöhelyi, A., Cserényi, J., and Solymosi, F., *J. Catal.* **141**, 287 (1993).
6. Erdöhelyi, A., Cserényi, J., Papp, E., and Solymosi, F., *Appl. Catal. A* **108**, 205 (1994).
7. Qin, D., and Lapszewicz, J., *Catal. Today* **21**, 551 (1994).
8. Nakamura, J., Aikawa, K., Sato, K., and Uchijima, T., *Catal. Lett.* **25**, 265 (1994).
9. Basini, L., and Sanfilippo, D., *J. Catal.* **157**, 162 (1995).
10. Rostrup-Nielsen, J. R., and Bak Hansen, J.-H., *J. Catal.* **144**, 38 (1993).
11. Rostrup-Nielsen, J. R., *in* "Natural Gas Conversion II" (H. E. Curry-Hyde and R. F. Howe, Eds.), Stud. Surf. Sci. Catal., Vol. 81, p. 25. Elsevier, Amsterdam, 1994.
12. Tsang, S. C., Claridge, J. B., and Green, M. L. H., *Catal. Today* **23**, 3 (1995).
13. Hu, Y. H., and Ruckenstein, E., *Catal. Lett.* **36**, 145 (1996).
14. Zhang, Z. L., and Verykios, X. E., *Catal. Today* **21**, 589 (1994).
15. Zhang, Z. L., and Verykios, X. E., *J. Chem. Soc. Chem. Commun.* **71**, (1995).
16. Ruckenstein, E., and Hu, Y. H., *Appl. Catal. A* **133**, 149 (1995).
17. Swaan, H. M., Kroll, V. C. H., Martin, and G. A., Mirodatos, C., *Catal. Today* **21**, 571 (1994).
18. Tang, S.-B., Qiu, F.-L., and Lu, S.-J., *Catal. Today* **24**, 253 (1995).
19. Choudhary, V. R., Uphade, B. S., and Mamman, A. S., *Catal. Lett.* **32**, 387 (1995).
20. Osaki, T., Horiuchi, T., Suzuki, K., and Mori, T., *Catal. Lett.* **35**, 39 (1995).
21. Rouhi, A. M., *Chem. Eng. News* **73**(22), 37 (1995).
22. Töpfer, H. J., *Gas Wasserfach* **117**, 412 (1976).
23. Teuner, S., *Hydrocarbon Proc.* **66**(7), 52 (1987).
24. Dibbern, H. C., Olesen, P., Rostrup-Nielsen, J. R., and Toettrup, P. B., *Hydrocarbon Proc.* **65**(1), 71 (1986).
25. Udengaard, N. R., Bak Hansen, J.-H., Hanson, D. C., and Stal, J. A., *Oil Gas J.* **90**(10), 62 (1992).
26. Ashcroft, A. T., Cheetham, A. K., Green, M. L. H., and Vernon, P. D. F., *Nature* **352**, 225 (1991).
27. Richardson, J. T., and Paripatyadar, S. A., *Appl. Catal.* **61**, 293 (1990).
28. Perera, J. S. H. Q., Couves, J. W., Sankar, G., and Thomas, J. M., *Catal. Lett.* **11**, 219 (1991).
29. Rostrup-Nielsen, J. R., *J. Catal.* **85**, 31 (1984).
30. Dumesic, J. A., Rudd, D. F., Aparicio, L. M., Rekoske, J. E., and Treviño, A. A., "The Microkinetics of Heterogeneous Catalysis," American Chemical Society, Washington, DC, 1993.
31. Wang, H.-Y., and Au, C.-T., *Catal. Lett.* **38**, 77 (1996).
32. Beebe, T. P., Jr., Goodman, D. W., Kay, B. D., and Yates, J. T., Jr., *J. Chem. Phys.* **87**, 2305 (1987).
33. Christmann, K., Schober, O., Ertl, G., and Neumann, M., *J. Chem. Phys.* **60**, 4528 (1974).
34. Hamza, A. V., and Madix, R. J., *J. Phys. Chem.* **89**, 5381 (1985).
35. Rendulic, K. D., Winkler, A., and Karner, H., *J. Vac. Sci. Technol. A* **5**, 488 (1987).
36. Rendulic, K. D., Anger, G., and Winkler, A., *Surf. Sci.* **208**, 4044 (1989).
37. Zhu, X.-Y., Akhter, S., Castro, M. E., White, J. M., *Surf. Sci.* **195**, L145 (1988).
38. Zhu, X.-Y., Castro, M. E., and White, J. M., *J. Chem. Phys.* **90**, 7442 (1989).
39. Chorkendorff, I., Alstrup, I., and Ullman, S., *Surf. Sci.* **227**, 291 (1990).
40. Ølgaard Nielsen, B., Luntz, A. C., Holmblad, P. M., and Chorkendorff, I., *Catal. Lett.* **32**, 15 (1995).
41. Siegbahn, P. E. M., and Panas, I., *Surf. Sci.* **240**, 37 (1990).
42. Burghgraef, H., Jansen, A. P. J., and van Santen, R. A., *Surf. Sci.* **324**, 345 (1995).
43. Underwood, R. P., and Bennett, C. O., *J. Catal.* **86**, 245 (1984).
44. Van Ho, S., and Harroit, P., *J. Catal.* **64**, 272 (1980).
45. Cant, N. W., and Bell, A. T., *J. Catal.* **73**, 257 (1982).
46. Efstathiou, A. M., and Bennett, C. O., *J. Catal.* **120**, 137 (1989).
47. Al-Sarraf, N., Stuckless, J. T., Wartnaby, C. E., and King, D. A., *Surf. Sci.* **283**, 427 (1993).
48. D'Evelyn, M. P., Steinrück, H.-P., and Madix, R. J., *Surf. Sci.* **180**, 47 (1987).
49. Kisinova, M. P., *Surf. Sci.* **111**, 584 (1981).
50. Tracy, J. C., *J. Chem. Phys.* **56**, 2736 (1972).
51. Xu, J., Ph.D. Thesis, University of Gent, Belgium, 1989.
52. Xu, J., and Froment, G. F., *AIChE J.* **35**, 88 (1989).
53. Haq, S., Love, J. G., Sanders, H. E., and King, D. A., *Surf. Sci.* **325**, 230 (1995).
54. Jones, T. S., Ashton, M. R., and Richardson, N. V., *J. Chem. Phys.* **90**, 7564 (1989).
55. Madix, R. J., Gland, J. L., Mitchell, G. E., and Sexton, B. A., *Surf. Sci.* **125**, 481 (1983).
56. Benzinger, J. B., and Madix, R., *Surf. Sci.* **79**, 394 (1979).
57. Askgaard, T. S., Nørskov, J. K., Ovesen, C. V., and Stoltze, P., *J. Catal.* **156**, 229 (1995).
58. Vannice, M. A., *J. Catal.* **44**, 152 (1976).
59. Goodman, D. W., Kelley, R. D., Madey, T. E., and Yates, J. T., Jr., *J. Catal.* **63**, 226 (1980).
60. Alstrup, I., *J. Catal.* **151**, 216 (1995).
61. van Hook, J. P., *Catal. Rev.-Sci. Eng.* **21**, 1 (1981).
62. Bodrov, I. M., Apel'baum, L. O., and Temkin, M. I., *Kinet. Katal.* **5**, 696 (1964).
63. Khomenko, A. A., Apel'baum, L. O., Shub, F. S., Snagovskii, Y. S., and Temkin, M. I., *Kinet. Katal.* **12**, 423 (1971).